C: Surfaces, Interfaces, Porous Materials, and Catalysis

2D Ni Nanoclusters on Ultrathin MgO/Ag(100)

Letizia Savio, Marco Smerieri, Jagriti Pal, Edvige Celasco, Mario Agostino Rocca, and Luca Vattuone

J. Phys. Chem. C, **Just Accepted Manuscript** • DOI: 10.1021/acs.jpcc.9b08684 • Publication Date (Web): 12 Dec 2019

2D Ni Nanoclusters on Ultrathin MgO/Ag(100)

Letizia Savio[1,], Marco Smerieri[1], Jagriti Pal[2,+], Edvige Celasco[1,2], Mario Rocca[1,2], Luca Vattuone[1,2]*

[1] IMEM-CNR, UOS Genova, Via Dodecaneso 33, 16146 Genova, Italy.

[2] Dipartimento di Fisica, Universita` di Genova, Via Dodecaneso 33, 16146 Genova, Italy

ABSTRACT:

Ni nanoclusters up to 30 Å in diameter are grown by Ni deposition on ultrathin MgO/Ag(100) films at different temperature and characterized by combining low temperature scanning tunnelling microscopy with photoemission and vibrational spectroscopies. At 200 K both small Ni_xO_y aggregates and 2D Ni nanoparticles of average size close to 12 Å form. The latter have a metallic nature and efficiently catalyze CO dissociation at 200 K. When Ni is deposited at 300 K, only larger 3D Ni clusters are observed.

Introduction

Metal nanoparticles (NPs) dispersed on metal oxide supports have been a matter of studies for decades due to their technological and industrial relevance for applications in fields such as sensoristics and heterogeneous catalysis [1,2]. In addition, they are considered as model systems able to bridge the so-called structure gap between single crystal surfaces [3], usually employed for a fundamental understanding of the reaction processes and identification of the active sites, and real catalysts, often consisting of oxides impregnated with (or supporting) nanoparticles of different size. The availability of size-selected clusters has further boosted research in this field by enabling to study the reactivity of nanoparticles for a selected reaction as a function of the number of atoms in the cluster [4].

In this frame, Ni NPs have been the subject of a particular attention both for their magnetic properties and for their high catalytic activity for economically relevant reactions such as methanation [5,6]. Indeed, Ni nanoclusters have been deposited on different oxide supports, including MgO [7–9], TiO_2 [10–13], $SrTiO_3$ [14] and Al_2O_3 [15]. In particular, due to its simple structure and wide bandgap, MgO became a model both as an active system in heterogeneous catalysis[16,17] and as a substrate for deposition of NPs. In fact, its non-reducible nature guarantees that it is a relatively inert support, though the edges of monolayer films were shown to dissociate water molecules [18,19]. On the other hand, the MgO substrate can influence the shape and size of the nanoparticles during their growth process and, consequently, affect their chemical reactivity.

In order to take advantage of electron based spectroscopies and imaging methods, usually thin or ultrathin oxide films deposited on metal supports are used in model studies. Large Ni NPs were deposited on a 10 ML film of MgO/Mo(001) [7]. At room temperature (RT), 1 ML-equivalent of Ni arranges in three dimensional (3D) NPs of 2 to 6 nm in diameter and 0.5 to 1.5 nm in height containing up to several hundred atoms. Due to the 16% lattice mismatch between the (100) face of MgO and the Ni fcc lattice, small Ni clusters take a hcp structure to reach commensurability with the MgO substrate and have interfacial Ni atoms in registry with surface oxygen atoms of the MgO layer. Only

for clusters larger than 2000 atoms in size, i.e. exceeding 4.5 nm in diameter and 2.5 nm in height, the fcc structure becomes energetically convenient with respect to the hcp one [20].

For nanoclusters of few Ni atoms on MgO(001), ab initio calculations predict a 3D shape already for the Ni_4 cluster [21], for which the tetrahedral configuration is proved to be most stable. In fact, since the binding energy.

of a single Ni atom onto the MgO surface is 1.4 eV [22,23] while the addition of a Ni atom to a pre-existing small Ni cluster is exothermic (by 2.6-4.1 eV, depending on the size of the cluster and the nature of the MgO site) the formation of large 3D clusters is energetically favoured. Surface energy arguments lead to the same conclusions; under equilibrium conditions, or at least when thermodynamics dominates over kinetics, the surface energy determines the growth mode of the cluster. For Ni, such quantity varies from 2.011 J/m^2 for Ni(111) to 2.368 J/m^2 for Ni(100) [24–26], while for MgO it is only 1.15 J/m^2 [27]. Therefore, when the mobility is high enough, formation of 3D clusters through a Vollmer Weber growth mode is expected.

At variance with this picture, if the mobility is not high enough to overcome the diffusion barriers, kinetics dominates over thermodynamics and 2D structures or small isolated clusters may form. For 0.03 ML of Ni deposited on Al_2O_3 at 300 K, e.g., 85 % of the NPs have an average diameter of 15 Å and an apparent height of 2-3 Å, reasonably corresponding to a single Ni layer. Only a minor fraction of the clusters shows a clear 3D shape [28]**.** Similarly, 0.1 ML of Ni deposited on ZrO_2/Pt_3Zr at RT leads to 90% of the clusters with apparent height lower than 2 Å, also compatible with a single layer of Ni atoms [29].

We showed that, if Ni is deposited on an ultra-flat monolayer MgO film at 200 K [30,31], the scenario can be even different [9]. At low (0.2 ML) Ni coverage, 2D nanoclusters of four to six atoms coexist with larger clusters. Both the shape and the interatomic distance between neighbouring Ni atoms of the former NPs are indicative of a non-metallic character consistent with Ni_yO_x aggregates [9]. The

spontaneous oxidation of NPs is enabled by the availability of oxygen atoms at the MgO/Ag interface; such atoms segregate to the surface through the MgO monolayer film, directly or - more probably - via an exchange mechanism involving the oxygen atoms of the MgO. In presence of Ni adatoms, these oxygens are captured to form the Ni_xO_y aggregates. DFT calculations allow to identify tetramers and pentamers with Ni_4O_5 and Ni_5O_{12} clusters, respectively. Therefore, under the investigated conditions, the formation of Ni_yO_x structures represents a competitive channel with respect to the growth of larger metallic Ni clusters. Indeed, the surface energy of NiO, calculated using ab initio methods, turns out to be 0.38 J/m^2 for (100), 0.82 J/m^2 for (110) and 1.14 J/m^2 for (111) surfaces [32] to be compared with the above given value of ~2 J/m^2 for bare Ni [24]. Therefore, if enough oxygen is available and its mobility is high enough, formation of Ni_xO_y is energetically favoured.

In the present work, we focus on Ni clusters grown on monolayer MgO and made of more than 6 Ni atoms. We demonstrate that they have a metallic nature and show how the deposition temperature affects their shape and size.

Experimental

Experiments were carried out in two different ultra-high vacuum apparatuses. The former consists of an analysis chamber, hosting a low temperature scanning tunneling microscope (LT-STM by Createc) and of a preparation chamber. The latter is equipped with a high resolution electron energy loss spectrometer (HREELS – Delta0.5 by SPECS) and with a conventional setup for X-ray Photoelectron spectroscopy (XPS - non monochromatized DAR400 Omicron X-ray source and EA125 Omicron hemispherical analyser).

Both UHV chambers are equipped with a Knudsen cell and an O_2 doser for reactive Mg evaporation, with a quartz microbalance (QMB) for Mg flux measurements, with an e-beam evaporator (Focus EFM 3) mounting a high purity (99.99%) Ni rod, with an ion-gun plus gas inlet for sample cleaning and with a quadrupole mass spectrometer for residual gas analysis. Finally, a four degrees of freedom

manipulator allows precise positioning of the sample holder in front of the preparation and analysis tools. The sample can be cooled by flowing liquid nitrogen through the sample holder.

The substrate is an Ag single crystal cut within 0.1° from the (100) plane. Before each experiment it was carefully cleaned by repeated cycles of sputtering with Ne^+ and annealing to T=850 K. Surface cleanliness and order were checked by STM or by XPS and LEED on either apparatus. Monolayer MgO films were grown by reactive deposition at T=773 K, followed by post-annealing in O_2 atmosphere (unless otherwise stated) and slow cooling to T<450 K, as detailed in ref. [31]. Mg was evaporated from a crucible heated to 593 K, providing an evaporation rate of ~1 Å/min. The background pressure of O_2 during Mg evaporation was kept at $P_{O2}=1\cdot10^{-6}$ mbar but, since a doser placed at ~2 cm from the Ag(100) surface was employed, an effective pressure at least 5 times higher is expected [33]. The MgO film thickness was evaluated *a priori* from the Mg flux estimated through the quartz microbalance and *a posteriori* by inspection of STM images and by quantitative analysis of the XPS spectra (see Supporting Material). The error assigned to the QMB is ±8%, while the Mg evaporation rate measured in different days under identical conditions is stable within 5%. We found an MgO coverage of 0.7 ML (in monolayers of Ag(100)) based on QBM calibration and of 0.83 ML based on XPS analysis. We consider the two estimates compatible taking into account the relative error on the QMB reading and on the calculated areas of XPS peaks (~10%). We will refer to this film as monolayer MgO in the following.

Ni was deposited on the MgO/Ag(100) sample at T=200 K using a commercial e-beam evaporator (Focus EFM 3) and always in a background pressure better than $2\ 10^{-9}$ mbar. The amount of Ni deposited is estimated a posteriori from the analysis of the STM images and of the XPS intensity for microscopy and spectroscopy experiments respectively (see Supporting Material). In the former case Ni clusters are found to cover approximately 10% of the total area of the substrate for the 100 K and 200 K preparations while in the latter we find a Ni/Mg concentration ratio of ~0.09. Therefore the agreement between the microscopic and spectroscopic sets of data is pretty fair.

Samples are cooled to T<150 K and inserted into the STM immediately after preparation.

STM images were recorded at liquid nitrogen temperature with a Pt/Ir tip cut in air under strain and then reshaped by controlled crashes into the surface, so that tunnelling occurs effectively through an Ag tip. The images were acquired in constant current mode, with typical tunnelling currents of ~0.2 nA and bias voltage applied to the sample -4.0 V<V<+4.0 V. The lateral size of the images and the orientation of the surface are determined from atomically resolved measurements of the clean Ag(100) surface; similarly, heights are calibrated on monatomic Ag steps. STM analysis was performed with the help of WSxM software [34].

XPS spectra were recorded at normal emission using the Al Kα emission line. The binding energy (E_b) was calibrated on the $Ag3d_{5/2}$ peak fixed at 368.25 eV [35]. The $Ni2p_{3/2}$ spectra were fitted using Voigt functions and a Shirley background. Three components were employed to take into account the possible oxidation states of Ni^0, Ni^{2+} and Ni^{3+}; a fourth component, shifted by 6 eV with respect to the Ni^0 binding energy and ascribed to the surface plasmon of metallic Ni in Ref. [36], is also added. HREEL spectra were recorded in-specular, at 62° incidence with respect to the surface normal and at primary electron energy E=4.0 eV to enhance the sensitivity to adsorbed species.

Results and Discussion

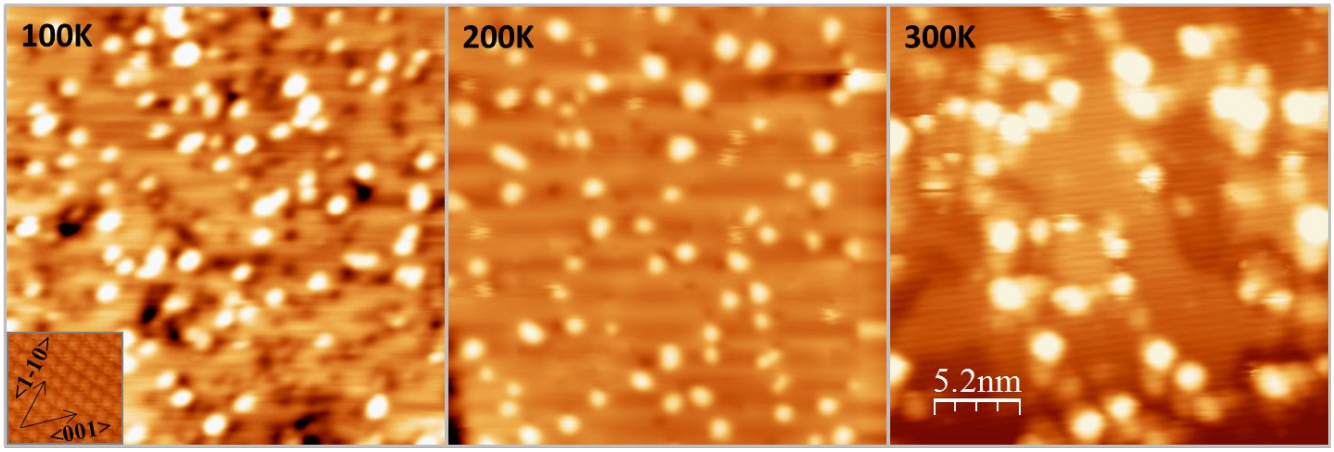

Figure 1. STM images of Ni nanoclusters on ML MgO/Ag(100) deposited at T=100K, 200K and 300 K. Image size (26x26) nm^2; V=+1.0 V. The inset in the bottom-left corner shows an atomically

resolved image of the clean Ag(100) substrate, used for calibration. For the 300 K preparation the MgO film was grown without post-annealing in O_2 pressure, therefore coalescence of islands with slightly different interface oxygen content are present (see Supporting Material). This approach allows to compare the behaviour of islands with different amount of interface oxygen with respect to the growth of 3D clusters.

Figure 1 shows STM images of Ni nanoclusters deposited on monolayer MgO/Ag(100) at three different deposition temperatures: a) 100 K , b) 200 K and c) 300 K. At RT, large and bright features decorate the borders of the MgO islands. At 100 K and 200 K, these features (*large* clusters in the following) are present in the middle of extended MgO terraces and coexist with smaller and fainter clusters. We have already identified the latter [9] as Ni_xO_y aggregates forming by spontaneous oxidation of Ni in presence of additional oxygen atoms available at the MgO/Ag interface. Since this bimodal distribution is more evident at 200 K, we deduce that this is the optimal temperature for the formation of Ni_xO_y aggregates, for which both some mobility of Ni adatoms and extraction of O atoms from the MgO/Ag interface are required.

Though the formation of the Ni_xO_y aggregates on the surface was important to clarify the role of the substrate in the determination of final geometry and composition of the clusters, these features represent a small fraction with respect to the total Ni coverage. Therefore, in the present work we focus on the characterization of the overall surface, discussing its morphology at different deposition temperature.

The size distribution of the clusters is reported in Figure 2 for the three investigated temperatures.

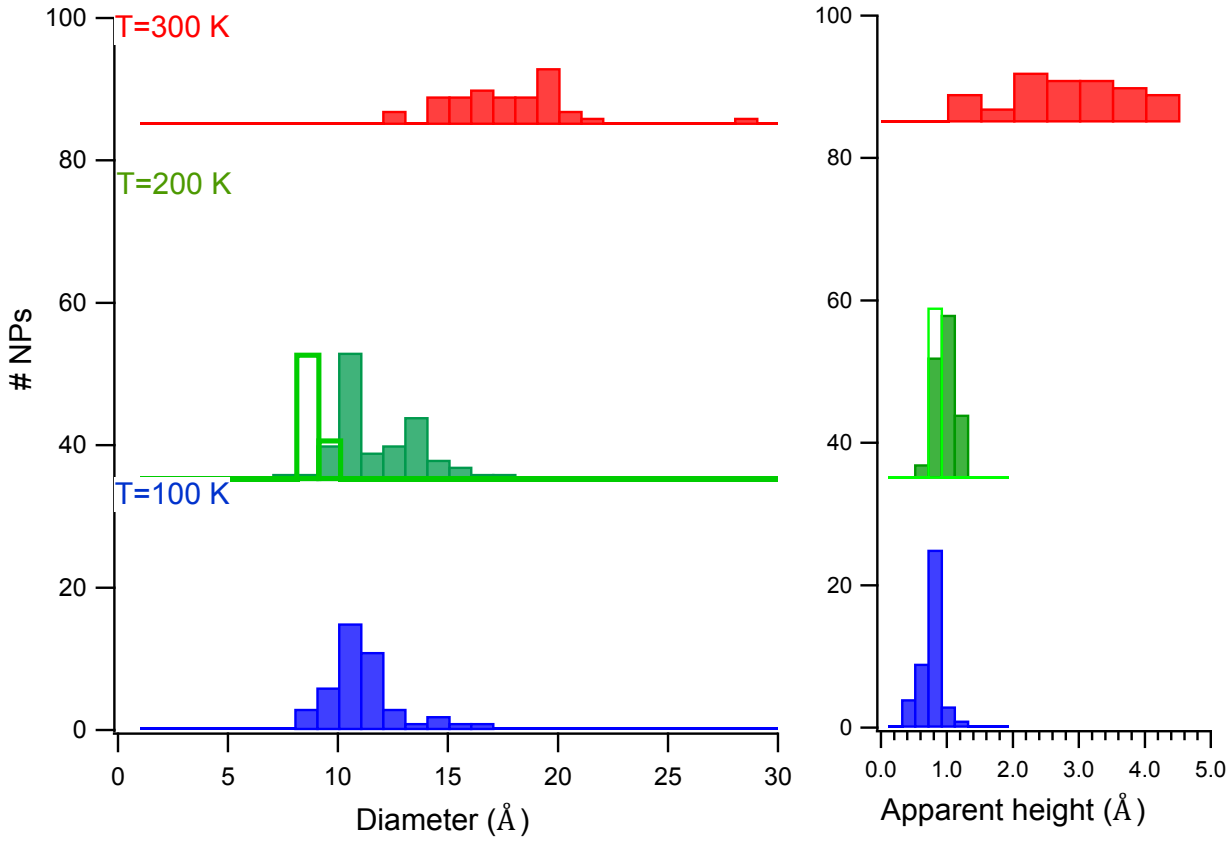

Figure 2. Size distribution of the nanoparticles at three different deposition temperatures: 300 K, 200 K and 100 K. At 200 K, the empty bars refer to the size distribution of Ni_xO_y aggregates (tetramers and pentamers), the filled ones to the dimensions of the large clusters.

We first note that:

1) The average diameter of the Ni clusters increases with deposition temperature, passing form an average value of (10.8±1.8) Å at 100 K to (11.6±2.1) Å at 200 K and to (17±3) Å at 300 K. While the first two values are compatible, the clusters forming at RT are considerably larger, indicating that a significant increase of the mobility of Ni adatoms sets in above 200 K.

2) The difference in the cluster size is reflected also on the height distributions reported in the right column of Figure 2. The average apparent height measured at V=1 V is (0.8±0.1) Å and

(1.0 ±0.2) Å for T=100 K and 200 K, respectively. This value reflects the electronic density of states and not the morphologic corrugation and depends on the applied bias, as shown in the bottom panels of Figure 3. However, by comparison with the apparent height measured from high resolution images of tetramers and pentamers [9] and with typical heights reported in literature for Ni clusters/films deposited on other oxide substrates [15,29], we deduce that the observed islands consist mainly of a single layer of Ni atoms. At 300 K, on the contrary, the height distribution is wider and shifted towards higher values; indeed the height distribution is almost flat between 2 Å and 4 Å. Between 200 K and 300 K interlayer diffusion becomes thus active, allowing for the growth of 3D clusters in order to minimize the free energy of the system, resulting in the aggregation of much larger, multilayered clusters containing up to tens of atoms.

3) Considering that the specific area for Ni(111) is 2.68 $Å^2$/atom, from the average size of the monolayer Ni clusters we can deduce that they are formed, on average, by (35±11) and (42±13) Ni atoms/cluster at 100 K and 200 K, respectively. The estimate for the 3D clusters obtained upon RT deposition is less reliable, and hence not given here, not only because of the slightly larger statistical error in their diameter but mainly because of their multilayer structure.

4) For T=200 K a bimodal distribution in the cluster size is evident. The larger clusters are sided by the small tetramers and pentamers, which present a much narrower size distribution (light green in the histogram of Figure 2) due to their well defined geometry. At this T, the population of larger clusters and of Ni_xO_y aggregates is approximately in a 2:1 ratio. A few Ni_xO_y structures are present also at 100 K, but in much smaller amount. However, a quantification is difficult in this case due to the slightly smaller size of the large clusters and to the lower resolution of the available STM images.

Since T=200 K corresponds to the condition for which the population of larger clusters and Ni_xO_y aggregates is best balanced on the surface and for which the images are better resolved, this is the optimal temperature for a comparative characterization of their behaviour.

Figure 3 shows the bias dependence of Ni nanoclusters deposited at T=200 K. Panels a) and b) report two sequences of STM images vs bias voltage, in which two large NPs and a tetramer are selected for further analysis. Panel c1) shows the line profile of the selected clusters at V=1.0 V and panel c2) displays their apparent height vs V.

The apparent height is lower for the tetramer than for the larger NPs. This effect can be explained by the oxide nature and therefore by the lower conductivity of the former. However, the contrast shows some bias dependence for both types of clusters. The tetramer apparent height reaches its maximum value of ~1 Å at V=1.0 V, and reduces monotonously to ~0.5 Å for V=±3.0 V. The larger clusters, on the contrary, show an almost constant height ~1.3 Å for -4.0 V ≤ V ≤ +2.0 V, which increases reaching 2.0 Å at V=4.0 V. Though the increase at 3.0 V is not of the same amount for the two NPs, which may be due to their conformation as well as to the quality of the tip, the behaviour is coherent for both NPs. It can be attributed to a change in the local density of states of the system, since at those voltages tunnelling occurs into the MgO conduction band [31,37]. The measured apparent height is close to the one calculated for the Ni-O distance for flat Ni clusters on MgO [38] and compatible with the values previously reported for monolayer islands of Ni on other metal oxides [28,29]. We can thus conclude that Ni deposition at T≤200 K leads to NPs of 1 ML thickness. The result is at variance with theoretical predictions which indicate the 3D geometry as the most stable form for Ni clusters of size n≥4, i.e. that Ni does not wet MgO(001) at equilibrium [22,38]. However, as discussed in the same ref. [38], the real situation for metal deposition on oxide layers may be more complex and affected by kinetic effects. E.g., if Cu is deposited on the ZnO(0001)–O surface at 130 K, it initially covers most of the surface in 2D islands [39] though it is predicted not to wet the surface according to thermodynamic considerations.

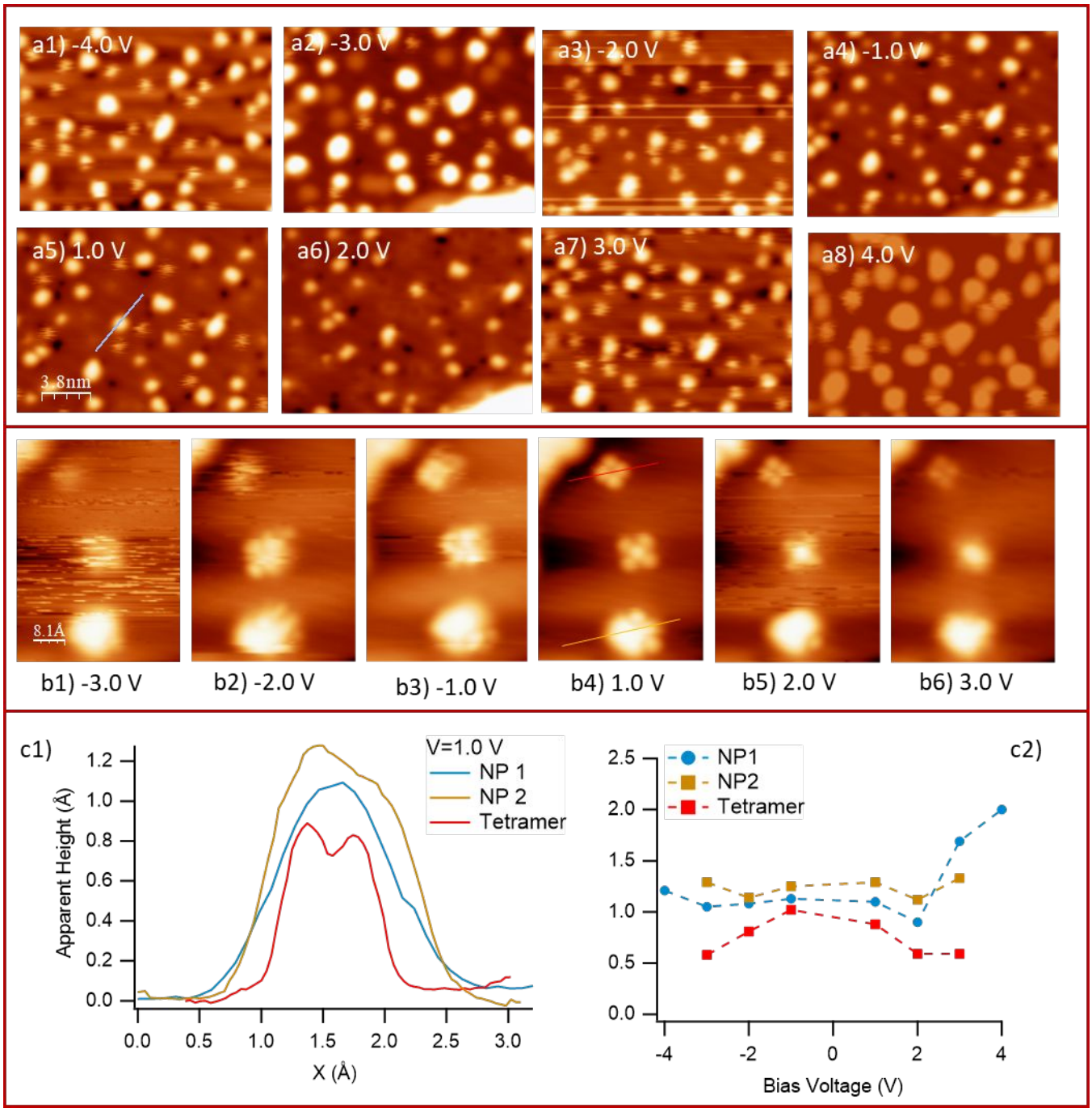

Figure 3. Series a) and b): STM images of Ni nanoclusters on ML MgO/Ag(100) deposited at 200K at different bias voltage. Panel c1): Line profile recorded at V=1.0 V for NP1 (marked by a line in a5), NP2 and a tetramer (both marked in b4). Panel c2): Variation of the apparent height vs bias voltage for the NPs of panel c1.

While the composition of tetramers and pentamers has been fully determined, the one of the larger NPs is not yet clear. In principle, due to the lower surface energy of NiO, it is reasonable that also a few Ni adatoms in larger clusters are bound to some segregated O atoms but we expect that the finite amount of oxygen available at the interface (at most ~0.3 ML according to ref.[30]) limits the extent of the oxidation of the Ni nanoparticles. Furthermore, the different types of NPs might be characterized by a different reactivity. To clarify these open issues, we performed XPS and HREELS analysis of the Ni/MgO/Ag(100) system obtained after Ni deposition at 200 K and exposure to CO at the same temperature. Both lower and higher temperatures were avoided in order to limit water contamination in the former case and to avoid coalescence or change of the morphology of the Ni clusters in the latter.

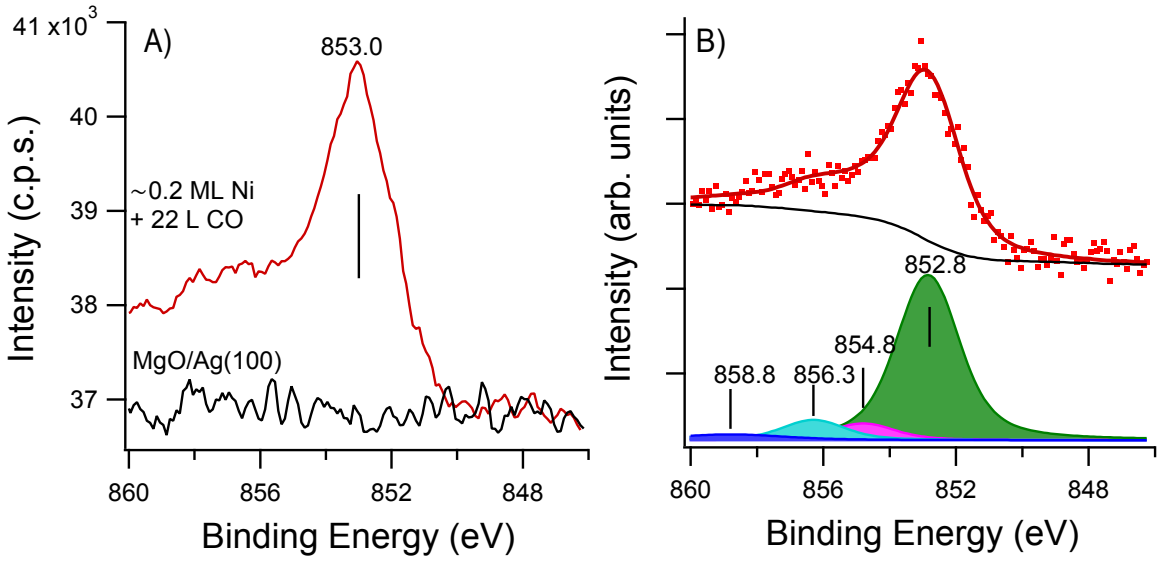

Figure 4. XPS spectrum recorded at a photon energy of 1486.6 eV after depositing Ni onto the surface at 200 K. Panel A) shows the raw Ni 2p spectrum in comparison with the bare MgO film. Panel B) reports the best fit to the data and the four components resolved after subtraction of a Shirley background.

A typical XPS spectrum of the Ni 2p region is reported in Figure 4A. The apparently simple shape of the Ni 2p line [36,40] is, in reality, quite complex to fit since it is composed of a different multiplet for each different Ni oxidation state. Fitting the $Ni2p_{3/2}$ line in Figure 4A with gaussian multiplets makes little sense due to the limited resolution of our non-monochromatic source; therefore we only consider a component for each different oxidation state of Ni, i.e. Ni^0 for metallic clusters and Ni^{2+} and Ni^{3+} as best approximation of the different Ni_xO_y stoichiometries of oxidized or partially oxidized clusters. For completeness, we also added a fourth, larger component corresponding to the main satellite peak of metallic Ni, which is expected at 6.0 eV higher than the corresponding main line.

By comparing the binding energy of the different components of our fit with those reported in ref.[36], it is straightforward to assign the line at 852.8 eV to metallic Ni and the ones at 854.8 and 856.3 eV to oxidized Ni in Ni^{2+} and Ni^{3+} states, respectively. From the relative peak areas, we estimate a population of 81%, 10% and 9% of Ni atoms in the Ni^0, Ni^{2+} and Ni^{3+} states, respectively. Considering that the average size of the large clusters is 11.6 Å and that their population is approximately double than the one of Ni_xO_y aggregates, we can calculate the ratio between the areas occupied by the two different kinds of structures, finding that the large NPs occupy 82% of the surface covered by Ni. Though this estimate may be affected by a significant error, due to the dispersion in cluster size, the good agreement with the fraction of Ni atoms in the metallic state is striking. We therefore conclude that Ni atoms in the large clusters are mainly metallic, with only a minor fraction of them being oxidized.

The interaction of the Ni NPs with CO was investigated to check whether it is possible to appreciate a different reactivity of the Ni nanoparticles and of the oxidized Ni_xO_y complexes from the analysis of the CO vibrational electron energy losses. The adsorption energy of CO on both MgO and NiO [41] is low enough to prevent stable CO adsorption at 200 K. Indeed, literature reports a stretch frequency for CO on NiO of ~ 267 meV after exposure at 80 K [42], i.e. very close to the gas phase value, indicating a weak interaction with this substrate. Moreover no CO can adsorb or react on bare Ag patches at this

temperature. Therefore, if CO adsorption occurs, it can be ascribed to interaction with the large metallic clusters only.

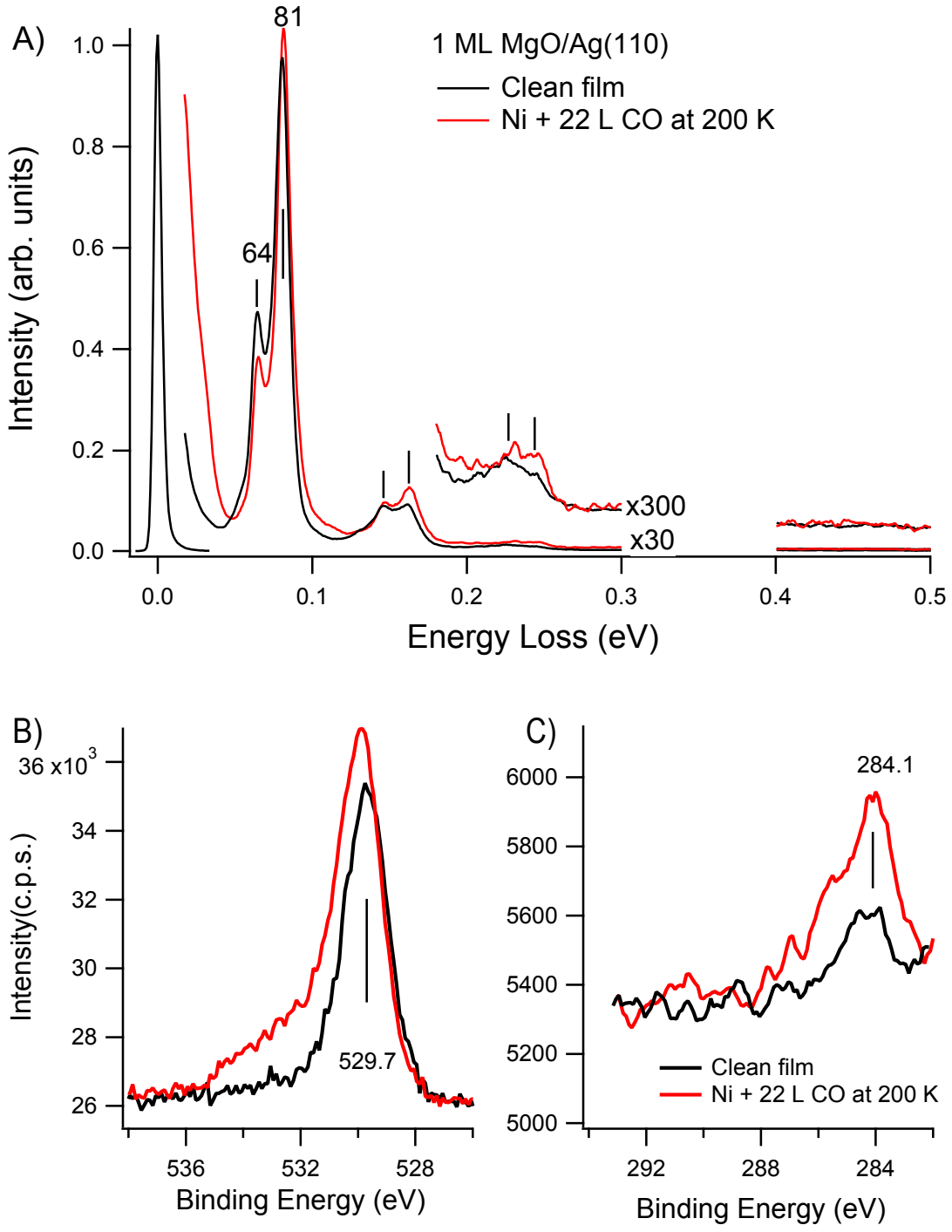

Figure 5. A) HREEL spectra recorded before (black) and after (red) Ni deposition (Ni/Mg concentration ratio of ~0.09) at 200 K and further exposure of the system to 22 L of CO at the same T. The thicks marked on the figure correspond to the position expected for overtones and combination

bands of the Fuchs-Kliewer modes and of the Wallis mode. Spectra are normalized to the inelastic background between 0.4 and 0.5 eV. B) and C): corresponding O1s and C1s region in the XPS spectrum.

The negative outcome of this experiment is summarized in Figure 5. Panel A shows the HREEL spectra corresponding to the clean MgO monolayer and to the same sample after deposition of Ni at 200 K followed by 22 L of CO exposure at the same temperature. Panels B and C report the corresponding O 1s and C 1s photoemission regions. The intense vibrational losses at 81 and 64 meV correspond to the Fuchs Kliewer related mode and to the Wallis mode of the MgO layer [31], while those of lower intensity correspond to their overtones and combination bands. CO adsorption experiments performed on selected mass clusters at 90 K showed CO related vibrations around 258, 237 and 171 meV, which U. Heiz et al.[4] assigned to top-bonded, bridge-bonded and "predissociated" CO (i.e. in the molecular precursor state to dissociation), respectively. The desorption temperature depends on cluster size but is always higher than 200 K so, if molecularly adsorbed CO were present, CO stretch vibrations around 250 meV would be expected in the HREEL spectra. No additional features are, however, evident in the spectra after the dose, indicating that CO adsorption is below our detection sensitivity under the present experimental conditions. Such behaviour suggests either that the amount of Ni is too low to yield a detectable HREEL signal or that CO dissociation occurs. The second hypothesis is supported by inspection of the photoemission data. In the O 1s region, the main O1s component at 529.7 eV grows and upshifts by 0.2 eV while the additional component at higher E_b becomes more intense. The C 1s region shows an increase of the peak at E_b~ 284 eV. We observe that the increase of both the C and O peaks cannot be related to any contamination occurring during the Ni deposition process, since it is not observed in a blank experiment preformed monitoring the sample without CO exposure (see Supporting Material). In the O 1s region, the shoulder at higher binding energy is most likely due to adsorbed water and/or OH coming from the background during

CO exposure. On the contrary, the increase of ~23% of the main O1s peak must be ascribed to O adatoms coming from CO dissociation. Such assignment is reinforced by estimating the corresponding increase of the C 1s signal at E_b suitable for C atoms resulting from CO dissociation, which is ~20% of the MgO coverage. The overall information suggests therefore that the amount of CO dissociated is larger than the Ni coverage itself. These findings can be rationalised only assuming that during CO uptake dissociation occurs yielding O and C atoms, which diffuse onto the surface leaving at least some active Ni sites where further CO molecules can dissociate. Coherently with this picture, no significant increase of the intensity around E_b=283.6 eV, i.e. at the binding energy of Ni_2C, is detected after CO exposure.

This finding is in agreement with the results reported in literature that CO dissociates efficiently at under-coordinated sites on Ni single crystals [43] and also with the presence of a desorption peak around 540-600 K due to associative desorption of CO after annealing mass selected Ni clusters [4]. The high efficiency of undercoordinated sites is proved also by the fact that dissociative CO chemisorption does not occur at low temperature on Low Miller Index Ni surfaces but it has been observed when decorating Rh steps with Ni atoms [44] and after deposition of Ni on Si [45]. As mentioned above, in the present work the average diameter of our Ni clusters deposited at 200 K is ~12 Å, corresponding to ~42 atoms/cluster. This implies that the majority of the Ni atoms in the cluster are at its edges. We can thus speculate that these under-coordinated sites are active for CO dissociation and their abundance explains the high dissociation efficiency observed in our experiment. Given the small Ni coverage and the reduced fraction of regular Ni sites within the 2D Ni NPs, the amount of molecularly adsorbed CO is probably below the detection limit of the HREEL spectrometer in the present experimental conditions.

These results demonstrate the catalytic potential for the 2D metallic nanoparticles obtained in the present study, while Ni_xO_y pentamers and tetramers are most probably totally inert under UHV conditions.

Conclusions

We have studied the initial stages of the deposition of Ni NPs on an ultrathin MgO/Ag(100) film by LT-STM, XPS and HREELS. The clusters shape and dimension depend on deposition temperature. In particular, at T=100 K and 200 K, 2D clusters forms. At 200 K, approximately 1/3 of them are small Ni_xO_y aggregates while the remaining 2/3 are metallic Ni clusters with an average diameter between 10 and 12 Å and of monoatomic in height. At 300 K the increased mobility of Ni allows for the formation of 3D clusters with an average size of 17 Å.

XPS analysis indicates that the amount of oxidized Ni atoms is compatible with the population of Ni_xO_y aggregates and hence that the larger clusters consist almost completely of metallic Ni atoms. The metallic NPs are active towards CO dissociation due to the high density of under-coordinated Ni atoms.

Corresponding Author

*corresponding author: letizia.savio@imem.cnr.it

Present Addresses

+ Fritz Haber Institute der Max Planck Gesellschaft, Faradayweg 4-6, 14195, Berlin, Germany.

Author Contributions

The manuscript was written through contributions of all authors. All authors have given approval to the final version of the manuscript.

Supporting Information

Supporting information describes how both MgO, Ni and C coverages were calculated and presents the blank experiment corresponding to the one of Figure 5.

Acknowledgments

Financial support from Università degli Studi di Genova through Fondo Ricerca di Ateneo 2018 is acknowledged.

References:

(1) Xu, C.; Goodman, D. W. Morphology and Local Electronic Structure of Metal Particles on Metal Oxide Surfaces: A Scanning Tunneling Microscopic and Scanning Tunneling Spectroscopic Study. *Chem. Phys. Lett.* **1996**, *263*, 13–18.

(2) Schneider, W.-D.; Heyde, M.; Freund, H.-J. Charge Control in Model Catalysis: The Decisive Role of the Oxide–Nanoparticle Interface. *Chem. – A Eur. J.* **2018**, *24*, 2317–2327.

(3) St.Clair, T. P.; Goodman, D. W. Metal Nanoclusters Supported on Metal Oxide Thin Films: Bridging the Materials Gap. *Top. Catal.* **2000**, *13*, 5–19.

(4) Heiz, U.; Vanolli, F.; Sanchez, A.; Schneider, W.-D. Size-Dependent Molecular Dissociation on Mass-Selected, Supported Metal Clusters. *J. Am. Chem. Soc.* **1998**, *120*, 9668–9671.

(5) Han, J. W.; Kim, C.; Park, J. S.; Lee, H. Highly Coke-Resistant Ni Nanoparticle Catalysts with Minimal Sintering in Dry Reforming of Methane. *ChemSusChem* **2014**, *7*, 451–456.

(6) Alstrup, I. On the Kinetics of CO Methanation on Nickel Surfaces. *J. Catal.* **1995**, *151*, 216–

225.

(7) Benedetti, S.; Myrach, P.; di Bona, A.; Valeri, S.; Nilius, N.; Freund, H.-J. Growth and Morphology of Metal Particles on MgO/Mo(001): A Comparative STM and Diffraction Study. *Phys. Rev. B* **2011**, *83*, 125423.

(8) Remar, D. F.; Turiev, A. M.; Tsidaeva, N. I.; Magkoev, T. T. Adsorption of Nitrogen Oxide Molecules to the Surface of Nanosized Nickel Clusters Formed on the (111) Surface of a Magnesium Oxide Film. *Russ. Phys. J.* **2010**, *53*, 480–485.

(9) Smerieri, M.; Pal, J.; Savio, L.; Vattuone, L.; Ferrando, R.; Tosoni, S.; Giordano, L.; Pacchioni, G.; Rocca, M. Spontaneous Oxidation of Ni Nanoclusters on MgO Monolayers Induced by Segregation of Interfacial Oxygen. *J. Phys. Chem. Lett.* **2015**, *6*, 3104–3109.

(10) Fujikawa, K.; Suzuki, S.; Koike, Y.; Chun, W.-J.; Asakura, K. Self-Regulated Ni Cluster Formation on the TiO2(110) Terrace Studied Using Scanning Tunneling Microscopy. *Surf. Sci.* **2006**, *600*, 117–121.

(11) Zhou, J.; Kang, Y. C.; Ma, S.; Chen, D. A. Adsorbate-Induced Dissociation of Metal Clusters: TiO2(110)-Supported Cu and Ni Clusters Exposed to Oxygen Gas. *Surf. Sci.* **2004**, *562*, 113–127.

(12) Tanner, R. E.; Goldfarb, I.; Castell, M. R.; Briggs, G. A. D. The Evolution of Ni Nanoislands on the Rutile TiO2(110) Surface with Coverage, Heating and Oxygen Treatment. *Surf. Sci.* **2001**, *486*, 167–184.

(13) Lai, X.; Clair, T. P. S.; Valden, M.; Goodman, D. W. Scanning Tunneling Microscopy Studies of Metal Clusters Supported on TiO2 (110): Morphology and Electronic Structure. *Prog. Surf. Sci.* **1998**, *59*, 25–52.

(14) Tanaka, M. Orientation-Dependent Growth of Ni Clusters on SrTiO3 (001), (110), and (111) Surfaces. *Jpn. J. Appl. Phys.* **2015**, *54*, 04DH09.

(15) Xu, C.; Lai, X.; Goodman, D. W. Local Electronic Structure of Metal Particles on Metal Oxide Surfaces: Ni on Alumina. *Faraday Discuss.* **1996**, *105*, 247.

(16) Philipp, R.; Fujimoto, K. FTIR Spectroscopic Study of Carbon Dioxide Adsorption/Desorption on Magnesia/Calcium Oxide Catalysts. *J. Phys. Chem.* **1992**, *96*, 9035–9038.

(17) Hu, Y. H.; Ruckenstein, E. BINARY MgO-BASED SOLID SOLUTION CATALYSTS FOR METHANE CONVERSION TO SYNGAS. *Catal. Rev.* **2002**, *44*, 423–453.

(18) Savio, L.; Celasco, E.; Vattuone, L.; Rocca, M. Enhanced Reactivity at Metal-Oxide Interface: Water Interaction with MgO Ultrathin Films. *J. Phys. Chem. B* **2004**, *108*, 7771–7778..

(19) Savio, L.; Celasco, E.; Vattuone, L.; Rocca, M. Enhanced Hydrolysis at Monolayer MgO Films. *J. Chem. Phys.* **2003**, *119*, 12053–12056.

(20) Ferrando, R.; Rossi, G.; Nita, F.; Barcaro, G.; Fortunelli, A. Interface-Stabilized Phases of Metal-on-Oxide Nanodots. *ACS Nano* **2008**, *2*, 1849–1856.

(21) Di Valentin, C.; Giordano, L.; Pacchioni, G.; Rösch, N. Nucleation and Growth of Ni Clusters on Regular Sites and F Centers on the MgO(001) Surface. *Surf. Sci.* **2003**, *522*, 175–184.

(22) Giordano, L.; Pacchioni, G.; Ferrari, A. M.; Illas, F.; Rösch, N. Electronic Structure and Magnetic Moments of Co4 and Ni4 Clusters Supported on the MgO(001) Surface. *Surf. Sci.* **2001**, *473*, 213–226.

(23) Neyman, K. M.; Inntam, C.; Nasluzov, V. A.; Kosarev, R.; Rösch, N. Adsorption of D-Metal Atoms on the Regular MgO(001) Surface: Density Functional Study of Cluster Models Embedded in an Elastic Polarizable Environment. *Appl. Phys. A* **2004**, *78*, 823–828.

(24) Vitos, L.; Ruban, A. V; Skriver, H. L.; Kollár, J. The Surface Energy of Metals. *Surf. Sci.*

1998, *411*, 186–202.

(25) Tyson, W. R.; Miller, W. A. Surface Free Energies of Solid Metals: Estimation from Liquid Surface Tension Measurements. *Surf. Sci.* **1977**, *62*, 267–276.

(26) Metals, C. in; Boer, F.R. de (Amsterdam Univ. (Netherlands)); Mattens, W.C.M. (Amsterdam Univ. (Netherlands)); Boom, R. (Hoogovens IJmuiden, IJmuiden (Netherlands)); Miedema, A.R. (Philips Research Laboratories, Eindhoven (Netherlands)); Niessen, A.K. (Philips Research, E. (Netherlands)). *Cohesion and Structure*; North-Holland: Amsterdam, 1988.

(27) Gibson, A.; Haydock, R.; LaFemina, J. P. Electronic Structure and Relative Stability of the MgO (001) and (111) Surfaces. *J. Vac. Sci. Technol. A* **1992**, *10*, 2361–2366.

(28) Zhi Xu; Surnev, L.; Uram, K. J.; Yates, J. T. Interactions Between Chemisorbed CO and Oxygen on Ni(111). *Surf. Sci.* **1993**, *292*, 235–247.

(29) Choi, J. I. J.; Mayr-Schmölzer, W.; Valenti, I.; Luches, P.; Mittendorfer, F.; Redinger, J.; Diebold, U.; Schmid, M. Metal Adatoms and Clusters on Ultrathin Zirconia Films. *J. Phys. Chem. C* **2016**, *120*, 9920–9932.

(30) Pal, J.; Smerieri, M.; Celasco, E.; Savio, L.; Vattuone, L.; Ferrando, R.; Tosoni, S.; Giordano, L.; Pacchioni, G.; Rocca, M. How Growing Conditions and Interfacial Oxygen Affect the Final Morphology of MgO/Ag(100) Films. *J. Phys. Chem. C* **2014**, *118*, 26091–26102.

(31) Pal, J.; Smerieri, M.; Celasco, E.; Savio, L.; Vattuone, L.; Rocca, M. Morphology of Monolayer MgO Films on Ag(100): Switching from Corrugated Islands to Extended Flat Terraces. *Phys. Rev. Lett.* **2013**, *112*, 1–5.

(32) Xiang, J.; Xiang, B.; Cui, X. NiO Nanoparticle Surface Energy Studies Using First Principles Calculations. *New J. Chem.* **2018**, *42*, 10791–10797.

(33) Henn, F. C.; Bussell, M. E.; Campbell, C. T. A Simple Means for Reproducibly Dosing Low Vapor Pressure and/or Reactive Gases to Surfaces in Ultrahigh Vacuum. *J. Vac. Sci. Technol. A Vacuum, Surfaces, Film.* **1991**, *9*, 10–13.

(34) Horcas, I.; Fernández, R.; Gómez-Rodríguez, J. M.; Colchero, J.; Gómez-Herrero, J.; Baro, A. M. WSXM: A Software for Scanning Probe Microscopy and a Tool for Nanotechnology. *Rev. Sci. Instrum.* **2007**, *78*, 013705.

(35) Powell, C. J. Elemental Binding Energies for X-Ray Photoelectron Spectroscopy. *Appl. Surf. Sci.* **1995**, *89*, 141–149.

(36) Grosvenor, A. P.; Biesinger, M. C.; Smart, R. S. C.; McIntyre, N. S. New Interpretations of XPS Spectra of Nickel Metal and Oxides. *Surf. Sci.* **2006**, *600*, 1771–1779.

(37) Schintke, S.; Messerli, S.; Pivetta, M.; Patthey, F.; Libioulle, L.; Stengel, M.; De Vita, A.; Schneider, W.-D. Insulator at the Ultrathin Limit: MgO on Ag(001). *Phys. Rev. Lett.* **2001**, *87*, 276801.

(38) Dong, Y. F.; Wang, S. J.; Mi, Y. Y.; Feng, Y. P.; Huan, A. C. H. First-Principles Studies on Initial Growth of Ni on MgO(001) Surface. *Surf. Sci.* **2006**, *600*, 2154–2162.

(39) Ernst, K. H.; Ludviksson, A.; Zhang, R.; Yoshihara, J.; Campbell, C. T. Growth Model for Metal Films on Oxide Surfaces: Cu on ZnO(0001)-O. *Phys. Rev. B* **1993**, *47*, 13782–13796.

(40) Biesinger, M. C.; Payne, B. P.; Lau, L. W. M.; Gerson, A.; Smart, R. S. C. X-Ray Photoelectron Spectroscopic Chemical State Quantification of Mixed Nickel Metal, Oxide and Hydroxide Systems. *Surf. Interface Anal.* **2009**, *41*, 324–332.

(41) Zaera, F. The Surface Chemistry of Heterogeneous Catalysis: Mechanisms, Selectivity, and Active Sites. *Chem. Rec.* **2005**, *5*, 133–144.

(42) Schönnenbeck, M.; Cappus, D.; Klinkmann, J.; Freund, H.-J.; Petterson, L. G. M.; Bagus, P. S. Adsorption of CO and NO on NiO and CoO: A Comparison. *Surf. Sci.* **1996**, *347*, 337–

345.

(43) Engbæk, J.; Lytken, O.; Nielsen, J. H.; Chorkendorff, I. CO Dissociation on Ni: The Effect of Steps and of Nickel Carbonyl. *Surf. Sci.* **2008**, *602*, 733–743.

(44) Stroppa, A.; Mittendorfer, F.; Andersen, J. N.; Parteder, G.; Allegretti, F.; Surnev, S.; Netzer, F. P. Adsorption and Dissociation of CO on Bare and Ni-Decorated Stepped Rh(553) Surfaces. *J. Phys. Chem. C* **2009**, *113*, 942–949.

(45) Asakawa, T.; Tanaka, K.; Toyoshima, I. Nickel Silicide Formation and Dissociative Adsorption of Carbon Monoxide on Nickel/Silicon (111) Studied by UPS and XPS. *J. Phys. Chem.* **1991**, *95*, 4783–4787.

TOC graphic

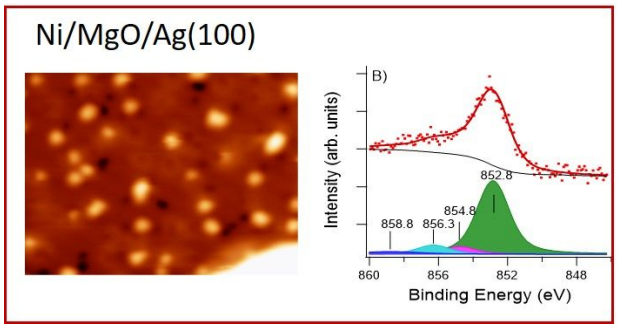
Ni/MgO/Ag(100)
B)
Intensity (arb. units)
852.8
854.8
858.8
856.3
860
856
852
848
Binding Energy (eV)